Extended abstract
25th Severe Local Storms Conf.
11-14 October 2010, Denver, CO

DUAL-DOPPLER WIND ANALYSIS OF CONVECTIVE STORMS USING THE VERTICAL VORTICITY EQUATION

Corey K. Potvin*[,1] and Alan Shapiro[1,2]
[1]School of Meteorology, University of Oklahoma, Norman, OK
[2]Center for Analysis and Prediction of Storms, University of Oklahoma, Norman, OK

1. INTRODUCTION

The vertical wind *w* is typically the most difficult component to retrieve in dual-Doppler wind analysis. Due to shallow beam elevation angles, *w* is the most poorly-sampled wind component in most radar scanning geometries. In addition, radial velocity data are often lacking near the ground due to earth curvature, non-zero base elevation angles, ground clutter contamination, beam blockage and rough terrain. Important information about low-level convergence/divergence is therefore often missing, resulting in significant errors in retrieved *w* at all levels even when the impermeability condition ($w = 0$) can be safely imposed at the ground. Finally, lack of radar coverage near storm top, where the vertical velocity field generally cannot be assumed to be zero (especially in developing convection) usually precludes application of an upper-level boundary condition on *w*. Because of these difficulties and the importance of the vertical velocity field in studies of convective dynamics and thermodynamics, accurate retrieval of *w* is a long-standing problem in dual-Doppler analysis.

The potential role of the vertical vorticity equation in improving mesoscale dual-Doppler retrievals of *w* has only recently been rigorously examined (Protat and Zawadzki 2000; Protat et al. 2001; Mewes and Shapiro 2002; Lee et al. 2003; Liu et al. 2005; Lee et al. 2006; Shapiro et al. 2009a). A new mesoscale dual-Doppler analysis technique was presented in Shapiro et al. (2009a), hereafter SPG09, that weakly (least-squares sense) satisfies the anelastic vertical vorticity equation in addition to data constraints, a mass conservation equation and smoothness constraints. In experiments with analytical wind fields containing strong low-level convergence/divergence, the vorticity constraint improved the retrieval of *w* (and low-level *u* and *v*) when pseudo-observations were withheld near the ground.

In the present study, the impact of the vorticity constraint is further explored using an Advanced Regional Prediction System (ARPS; Xue et al. 2001) simulation of a supercell thunderstorm. Several improvements to the original SPG09 technique are described and their impacts on the analyses examined. These modifications are primarily designed to account for flow unsteadiness.

Due to the typically long intervals (1-5 min) between radar volume scans in operational and some research settings, direct computation of the local vorticity derivative may produce large discretization errors in cases where portions of the wind field are rapidly moving. The local derivative was therefore evaluated in SPG09 using a frozen-turbulence space-time transformation that necessitates estimates of the pattern-translation components *U* and *V*. Experiments in SPG09 revealed that the success of the vorticity constraint can be significantly diminished (or even reversed) by large errors in these estimates. Given that the advection velocity field is often highly spatially-inhomogeneous in the presence of vigorous convection, it seems likely that the use of spatially-constant *U* and *V* in the vorticity constraint could introduce significant errors into the analysis (especially of *w*). Thus, in the present study, a recently-developed pattern-translation retrieval method that allows for spatially-variable *U*

* Corresponding Author Address: Corey Potvin, 120 David L. Boren Blvd, Room 4355, Norman, OK 73072; email: corey.potvin@noaa.gov.

and *V* (Shapiro et al. 2010) is used. The use of spatially-variable *U* and *V* should also improve the impact of the data constraint, which uses these estimates to extrapolate parcel locations to the analysis time.

Advection-correction addresses only one source of wind field unsteadiness, namely, translation. Failure to account for intrinsic (Lagrangian) evolution of the horizontal wind field between the analysis time and the times at which observations are valid can also degrade the retrieval, especially in the presence of developing or decaying convection. In this study, we examine the impact of including estimates of the Lagrangian tendencies of the horizontal wind components and vertical vorticity in the data and vorticity constraints, respectively. These estimates are obtained from two provisional wind retrievals performed prior to the final dual-Doppler analysis. We are especially interested in the impact of the intrinsic vorticity evolution estimates since large errors in the local vorticity tendency term can significantly limit the effectiveness of the vorticity constraint.

The rest of this paper is organized as follows. The updated analysis procedure is described in Section 2, with emphasis placed on the recent improvements (interested readers are referred to SPG09 for additional discussion of the original cost function formulation). Experiments with pseudo-observations generated from the high-resolution ARPS supercell simulation are presented in Section 3. A summary and plans for future work follow in Section 4.

2. METHODOLOGY

2.1. Updated cost function formulation

As in SPG09, the analyzed Cartesian wind components $u^a(x, y, z)$, $v^a(x, y, z)$ and $w^a(x, y, z)$ are obtained in this study by minimizing a cost function *J* that quantifies violations of data, mass conservation, vorticity and smoothness constraints. However, in many of the experiments below, *J* is modified to include pre-calculated estimates of the Lagrangian evolution of the horizontal winds, D^*u/Dt^* and D^*v/Dt^*, and of the vertical vorticity, $D^*\zeta/Dt^*$. These estimates are computed from provisional dual-Doppler analyses of two consecutive volume scans (more details later). As in SPG09, however, only velocity data from a single (dual-Doppler) volume scan are explicitly used in the final dual-Doppler analysis. *J* is also modified in some experiments to use second-order rather than first-order derivatives in the spatial smoothness penalty terms.

The calculation of the modified *J* is now described, with details of the estimation of the wind field translation and evolution deferred until the end of this section. As in the original approach, the modified *J* is a sum of individual *J*'s associated with various constraints. In each of these cost functions, the (constant) constraint weight is represented by a subscripted λ. The observational cost function

$$J_O \equiv \sum_{Rad1} \lambda_{O1}\, r_1^2 \left(v_{r1}^{obs} - v_{r1}^{a}\right)^2 + \sum_{Rad2} \lambda_{O2}\, r_2^2 \left(v_{r2}^{obs} - v_{r2}^{a}\right)^2$$

sums the range-weighted root-mean-square (RMS) differences between the observed and analyzed radial winds over the observational spaces of two radars, Rad1 and Rad2 (the formulation could easily be extended to three or more radars). Using the first radar for illustration, r_1 is the distance from Rad1 to a radial wind observation v_{r1}^{obs}. The spatial locations of v_{r1}^{obs} are transformed from the spherical coordinates to the Cartesian coordinates. We let (*x*, *y*, *z, t*) denote the parcel collocated with v_{r1}^{obs} at the observation time *t*. In order to account for the translation of this parcel between the analysis time (t=0) and *t*, the analyzed radial wind v_{r1}^{a} is computed from the u^a, v^a and w^a evaluated at the backward-advected parcel location given by:

$$(x^*, y^*, z^*, 0) = \left(x - U(x,y,z)t,\ y - V(x,y,z)t,\ z,\ t\right) \quad (1)$$

where *U* and *V* are the pre-calculated advection velocity components. This space-time transformation is valid to the extent that Taylor's (1939) frozen-turbulence hypothesis is satisfied by the observed reflectivity fields and that the reflectivity is a marker of the air flow. The analyzed wind components as well as the pre-calculated horizontal wind evolution estimates *D*u/Dt** and *D*v/Dt** are interpolated to the backward-advected parcel locations (*x**, *y**, *z**) using the Cressman (1959) method with a 500 m cutoff radius. The analyzed radial wind is calculated as:

$$v_{r1}^{a} = \hat{r}_1(x,y,z) \bullet \left\{ \left[u^a(x^*,y^*,z^*) + t\frac{D^*u}{Dt^*}(x^*,y^*,z^*) \right]\hat{i} + \left[v^a(x^*,y^*,z^*) + t\frac{D^*v}{Dt^*}(x^*,y^*,z^*) \right]\hat{j} + \left[w^a(x^*,y^*,z^*) - |w_t| \right]\hat{k} \right\}$$

where w_t is the estimated terminal velocity of hydrometeors relative to the air (e.g. Shapiro et al. 1995), set to zero in this study since the ARPS *w* describes vertical air (not scatterer) motion, and

$$\hat{r}_1(x,y,z) = (\cos\theta\sin\phi)\hat{i} + (\cos\theta\cos\phi)\hat{j} + (\sin\theta)\hat{k}$$

is the radial (with respect to Rad1) unit vector given the azimuth angle ϕ and elevation angle θ of the radar beam.

The anelastic mass conservation cost function is unchanged from SPG09 and is expressed by

$$J_M \equiv \sum_{\text{Cart}} \lambda_M \left[\frac{\partial(\rho_s u^a)}{\partial x} + \frac{\partial(\rho_s v^a)}{\partial y} + \frac{\partial(\rho_s w^a)}{\partial z} \right]^2$$

where the base-state atmospheric density $\rho_s(z)$ profile is assumed in this study to be

$$\rho_s(z) = \rho_0 e^{-\frac{z}{H}}$$

with reference density ρ_o and scale height *H*=10 km. This and the remaining cost functions are computed over the Cartesian analysis grid (Cart).

The anelastic vertical vorticity equation used in the analysis procedure is:

$$\frac{\partial\zeta}{\partial t} + \vec{u}\cdot\nabla\zeta + \left(\frac{\partial v}{\partial z}\frac{\partial w}{\partial x} - \frac{\partial u}{\partial z}\frac{\partial w}{\partial y} \right) + \zeta\left(\frac{\partial u}{\partial x} + \frac{\partial v}{\partial y} \right) = 0 \quad (2)$$

where the vertical vorticity $\zeta \equiv \partial v/\partial x - \partial u/\partial y$ and $\vec{u}$ is the 3-D wind vector. Justification for the use of this approximated vorticity equation in mesoscale convective flows is given in SPG09. As in that study, we do not seek to compute the local vorticity derivative directly since this may introduce large temporal discretization errors. Instead, consider the total vorticity derivative in the moving reference frame used in (1):

$$\frac{D^*\zeta}{Dt^*} = \frac{\partial\zeta}{\partial t} + \vec{U}\cdot\nabla\zeta ,$$

where $\vec{U}$ is the horizontal advection velocity. Rearranging terms,

$$\frac{\partial\zeta}{\partial t} = \frac{D^*\zeta}{Dt^*} - \vec{U}\cdot\nabla\zeta .$$

Substituting for the local derivative in (2), we obtain:

$$\frac{D^*\zeta}{Dt^*} + (\vec{u}-\vec{U})\cdot\nabla\zeta + \left(\frac{\partial v}{\partial z}\frac{\partial w}{\partial x} - \frac{\partial u}{\partial z}\frac{\partial w}{\partial y} \right) + \zeta\left(\frac{\partial u}{\partial x} + \frac{\partial v}{\partial y} \right) = 0 .$$

In SPG09, only the contribution of the wind field translation to the local vorticity tendency was considered; that is, $D^*\zeta/Dt^*$ was implicitly set to zero. In the present study, however, we also make provision for this Lagrangian vorticity evolution. The new vorticity constraint can therefore be expressed as:

$$J_V \equiv \sum_{Cart} \lambda_V \left[\frac{D\zeta^*}{Dt^*} + (u^a - U)\frac{\partial \zeta^a}{\partial x} + (v^a - V)\frac{\partial \zeta^a}{\partial y} + w^a \frac{\partial \zeta^a}{\partial z} + \left(\frac{\partial v^a}{\partial z}\frac{\partial w^a}{\partial x} - \frac{\partial u^a}{\partial z}\frac{\partial w^a}{\partial y} \right) + \zeta^a \left(\frac{\partial u^a}{\partial x} + \frac{\partial v^a}{\partial y} \right) \right]^2 .$$

Finally, the smoothness cost function is the same as that used in SPG09:

$$J_S \equiv \sum_{Cart} \lambda_{S1} \left[\left(\frac{\partial u^a}{\partial x} \right)^2 + \left(\frac{\partial u^a}{\partial y} \right)^2 + \left(\frac{\partial v^a}{\partial x} \right)^2 + \left(\frac{\partial v^a}{\partial y} \right)^2 \right] + \sum_{Cart} \lambda_{S2} \left[\left(\frac{\partial u^a}{\partial z} \right)^2 + \left(\frac{\partial v^a}{\partial z} \right)^2 \right]$$
$$+ \sum_{Cart} \lambda_{S3} \left[\left(\frac{\partial w^a}{\partial x} \right)^2 + \left(\frac{\partial w^a}{\partial y} \right)^2 \right] + \sum_{Cart} \lambda_{S4} \left(\frac{\partial w^a}{\partial z} \right)^2 .$$

J_S penalizes small-scale noise in the analyzed wind field.

The analysis (control) variables $u^a(x, y, z)$, $v^a(x, y, z)$, $w^a(x, y, z)$ are obtained by minimizing J using the Polak-Ribiere conjugate gradient method (Press et al. 1992). A first guess of zero is used for all the control variables. The minimization procedure is considered to have converged once the change in u (in the two provisional retrievals, described below) or w (in the final retrieval) over ten iterations of the procedure is everywhere less than .02 m s^{-1}.

2.2. Advection correction

The advection velocity field can be highly spatially-inhomogeneous in the presence of severe convection, where features in different locations (e.g. left- and right-supercell pair) or having different scales (e.g. tornado rotating around a mesocyclone) often move at very different velocities. Thus, in this study, the pattern translation velocity is estimated using a recently-developed advection-correction method that makes provision for spatially-variable translation components $U(x, y, z)$, $V(x, y, z)$ (Shapiro et al. 2010). The method is designed to operate on constant-height or constant-elevation-angle analyses of reflectivity or radial velocity valid at two different times. The retrieved (U, V) at each analysis level weakly satisfies the frozen-turbulence hypothesis and a smoothness constraint. In this study, Constant Altitude Plan Position Indicator (CAPPI) analyses of reflectivity are used. Reflectivity values < 0 dBZ are rejected in order to mitigate the effect of noise on the advection velocity retrieval.

In our experiments, reflectivity CAPPIs valid at each of the analysis levels for two consecutive volume scans (labeled Vol1 and Vol2) are input to the advection retrieval procedure. Vol1 begins at t=0, the time at which the final dual-Doppler analysis is valid. Vol2 immediately follows Vol1 and begins at t=T. Radial velocity data from both Vol1 and Vol2 are used to calculate D^*u/Dt^*, D^*v/Dt^* and $D^*\zeta/Dt^*$; however, only velocity observations from Vol1 are directly input to the observational cost function. The retrieved reflectivity translation field (U, V) is then used as a proxy for the translation of the Cartesian wind and vorticity fields. In data-denial experiments, (U, V) at levels below the data cutoff are set equal to the retrieved (U, V) at the data cutoff. We note that though the space-time correction (1) used to extrapolate

provisional u, v and w values to the analysis time does not account for variations in U and V along parcel trajectories, the loss of accuracy is minimal since these variations will typically be small due to the relatively smooth U, V fields produced by the advection retrieval procedure.

2.3. Wind and vorticity evolution estimation

The evolution estimates D^*u/Dt^*, D^*v/Dt^* and $D^*\zeta/Dt^*$ are calculated from two provisional horizontal wind retrievals valid at the beginnings of Vol1 (u_1, v_1) and Vol2 (u_2, v_2). (The vertical wind component is also retrieved but is not used in the evolution estimation). The vertical vorticity fields ζ_1 and ζ_2 are computed from the two horizontal wind fields. The vorticity constraint is not imposed during the provisional retrievals since u, v can be accurately retrieved using just the data, mass conservation and smoothness constraints, and since including the vorticity constraint with $D^*\zeta/Dt^* \equiv 0$ could degrade the retrieval.

To calculate the evolution estimates, the positions of hypothetical parcels located at each of the analysis grid points at the beginning of Vol1 (x_1, y_1, z_1, 0) are tracked to the beginning of Vol2 as follows: (x', y', z', t') = (x_1+U^*T, y_1+V^*T, z_1, T). The estimated u, v and ζ for each parcel at t=T, (u', v' and ζ'), are then interpolated from the u_2, v_2 and ζ_2 fields. Next, the evolution estimates are calculated: $D^*u/Dt^*(x_1, y_1, z_1) = (u'-u_1)$/T, $D^*v/Dt^*(x_1, y_1, z_1) = (v'-v_1)$/T, $D^*\zeta/Dt^*(x_1, y_1, z_1) = (\zeta'-\zeta_1)$/T. Finally, a nine-point 2-D smoother is applied to the fields in order to mitigate noise.

There are three important potential sources of error in these wind and vorticity evolution estimates. These are nonlinear evolution of the wind field, inaccurate (U, V), and the use of linear extrapolation rather than a numerical integration method (e.g. Runge-Kutta) to estimate the locations of parcels at t=T. However, given the volume scan times this technique is primarily designed for (~2 min or less), the resulting errors in D^*u/Dt^*, D^*v/Dt^* and $D^*\zeta/Dt^*$ should generally be small enough that using these estimates either improves or has little impact on the retrieval of u^a, v^a and w^a. This hypothesis is supported by the tests presented below.

3. EXPERIMENTS WITH ARPS SUPERCELL SIMULATION

3.1. Description of simulation

The dual-Doppler technique was tested using a very high-resolution ARPS simulation of a supercell. This facilitated verification of analyses (since the true u, v and w fields are known) while providing a more realistic test of the technique than the analytical tests in SPG09. The model thunderstorm was initiated by a thermal bubble placed in a homogeneous environment defined by a sounding proximate to the 20 May 1977 Del City, Oklahoma supercell storm. Computations were performed over a 48 km × 48 km domain with 25 m horizontal grid spacing and vertical grid spacing increasing from 20 m at the surface to about 80 m at 1 km AGL to 380 m at 16 km AGL. The integration proceeded in a translating reference frame chosen to maintain the parent storm near the domain center throughout the duration of the simulation. The Kessler-type warm rain microphysics was used. The model fields used in our retrieval experiments begin 3.5 h into the simulation. The simulated storm exhibits many commonly-observed supercell features including a mesocyclone and associated strong central updraft, a hook echo signature, and a rear-flank downdraft (Fig. 1).

3.2. Analysis domains

The (final) dual-Doppler analyses were performed over a 20-km X 20-km X 6-km subdomain of the ARPS simulation. This subdomain has 500-m grid spacing in all three dimensions, and is henceforth referred to as the “final analysis domain”. The provisional dual-Doppler analyses and advection velocity retrieval proceeded over a larger, 36-km by 36-km domain (henceforth “provisional analysis domain”) that enclosed

the final analysis domain. The lower-left corner of the provisional analysis domain is the origin of the Cartesian coordinate system used in these experiments.

3.3. Radial velocity and reflectivity emulation

Emulated radars positioned at (x = -7.5 km, y = -13 km, z = 0 km) and (x = 42.5 km, y = -13 km, z = 0 km) performed volume-sector scans of the provisional analysis domain. The radar and analysis domains are depicted in Fig. 2. Radar scans were performed at elevation angles extending from 0.5° to 16.5° in 1° increments. Range and azimuthal intervals of 200 m and 1°, respectively, were used. The volume scan time was generally set to 1 min, but was increased to 2 min in several experiments. The emulated radial velocity observations were generated by Cressman-interpolating (cutoff radius = 500 m) the ARPS u, v and w to each radar grid point and taking the radial (with respect to the radar) component. Reflectivity pseudo-observations were computed using the same interpolation procedure as in the radial velocity emulation. The reflectivity (dBZ) values R used to create both the reflectivity pseudo-observations (though Cressman interpolation from the ARPS to the radar domain) and the CAPPIs were calculated by

$$R = 10\log_{10}\left(3.631\times10^{9} q_r^{1.75}\right)$$

where q_r is the model rainwater mixing ratio (kg kg^{-1}) vertically-interpolated to the analysis domain. Emulated radial velocities associated with emulated reflectivity < 5 dBZ were omitted from the analysis in order to imitate the unavailability of real Doppler velocities in regions of low signal-to-noise ratio.

Since we are primarily concerned with the scenario where radar data coverage near the surface is lacking, radar pseudo-observations below 1.5 km AGL were withheld from the analysis. Consequently, *D*u/Dt*, D*v/Dt* and D*ζ/Dt** were set to zero at and below the data cutoff, and U and V within the data void were set to their retrieved values at z = 1.5 km.

3.4. Analysis verification

The "true" u, v, and w fields used to verify the dual-Doppler analyses were generated by downscaling the ARPS wind component values to the analysis grid using Cressman interpolation with a 500 m cutoff radius. Root-mean-square (RMS) errors in u^a, v^a and w^a were calculated for each analysis level. In order to focus the verification on regions where data were available (prior to rejection of data below 1.5 km), only analysis points located within 500 m of an emulated reflectivity value > 5 dBZ were used in the RMS error calculations.

*3.5. Impact of D*u/Dt*, D*v/Dt* and D*ζ/Dt**

In all the experiments that follow, the data, mass conservation and smoothness constraints were turned on, and the impermeability condition was exactly satisfied at the surface. The vorticity constraint was alternately turned on (VORT) or off (NOVORT). In preliminary experiments, including *D*u/Dt** and *D*v/Dt** in the data constraint did little or nothing to improve the retrieval of u, v and w, and so these estimates were not used in the experiments presented below. The failure of the horizontal wind evolution estimates to improve the analysis will be investigated in future work. Including *D*ζ/Dt** in the vorticity constraint, on the other hand, reduced the RMS error in w by ~10-15 % at each level above the data void. The vorticity evolution estimates were therefore used in all of the VORT experiments described below.

3.6. Impact of vorticity constraint

Including the vorticity constraint in the dual-Doppler analysis significantly improved the retrieval of w at all analysis levels, even within the data void (Fig. 3). The RMS errors in w in VORT relative to NOVORT were reduced by ~20-35 % at each level, with the greatest improvements away from the top and bottom of the domain. Horizontal and vertical

cross-sections of the retrieved *w* fields reveal that the vorticity constraint had the largest impact on the stronger updrafts (Figs. 4, 5). As was the case with the analytical experiments performed in SPG09, much of the improvement in the retrieved *u* and *v* occurred below the data cutoff (Fig. 6). In a separate set of experiments in which radar data were not rejected below a certain level (not shown), the improvement in the *w* retrieval in VORT relative to NOVORT was significantly reduced. This is presumably due to the fact that much of the low-level horizontal divergence was recovered using NOVORT, thus diminishing the need for the vorticity constraint. All of these results indicate that the vorticity constraint is capable of transporting useful dynamical information into regions where radar data are unavailable.

The VORT and NOVORT retrievals were repeated using a 2 min volume scan time (Fig. 3). Consistent with the analytical experiments in SPG09, doubling the volume scan time degraded the VORT *w* retrieval more than the NOVORT retrieval. This is because the contributions of *U*, *V* and $D^*\zeta/Dt^*$ to the local vorticity derivative become more error-prone as the time interval over which these parameters are calculated increases. However, the vorticity constraint still significantly improved the *w* retrieval, with RMS errors being reduced by ~18-30 % at each level.

3.7. Impact of 3-D advection correction

In order to assess the value added by accounting for wind field translation in the dual-Doppler analysis, the VORT and NOVORT experiments were repeated without advection correction ($U=V=0$). The VORT (NOVORT) *w* retrieval was generally degraded by < 5 % (< 1 %) at each level. The changes in *u* and *v* in both VORT and NOVORT were generally < 1%. The insignificance of the impact of the *U* and *V* estimates in this case is likely partly attributable to the fact that the ARPS simulation was performed in a moving reference frame in order to keep the storm near the domain center.

4. SUMMARY AND FUTURE WORK

Encouraged by the results in SPG09, we have continued to explore the capability of the anelastic vertical vorticity constraint to improve variational dual-Doppler vertical wind retrieval in convective storms when low-level radar coverage is lacking. The use of a realistic numerical supercell simulation in the present study permitted a rigorous and straightforward assessment of our technique. The vorticity constraint significantly improved vertical velocity retrievals in our experiments, with much of the improvement resulting from the transmission of dynamical information into the radar data void. Accounting for the Lagrangian evolution of the vertical vorticity field significantly increased the utility of the vorticity constraint.

The dual-Doppler technique will next be tested using real radar observations of convective storms. These tests will hopefully permit a more representative assessment of the utility of spatially-variable advection correction in rapidly-translating convective flows.

Acknowledgments. This research was supported by the National Science Foundation (NSF) under Grant ATM-0532107 and by the Engineering Research Centers Program of the NSF under Cooperative Agreement EEC-0313747.

References

Cressman, G. P., 1959: An operational objective analysis system. *Mon. Wea. Rev.,* **87,** 367–374.

Lee, Y.-H. Kuo, and A. E. MacDonald, 2003: The vorticity method: Extension to mesoscale vertical velocity and validation for tropical storms. *Quart. J. Roy. Meteor. Soc.*, **129**, 1029–1050.

——, W. C. Lee, and A. E. MacDonald, 2006: Estimating vertical velocity and radial flow from Doppler radar observations of

tropical cyclones. *Quart. J. Roy. Meteor. Soc.*, **132**, 125–145.

Liu, S., C. Qiu, Q. Xu, P. Zhang, J. Gao, and A. Shao, 2005: An improved method for Doppler wind and thermodynamic retrievals. *Adv. Atmos. Sci.*, **22**, 90–102.

Mewes, J. J., and A. Shapiro, 2002: Use of the vorticity equation in dual-Doppler analysis of the vertical velocity field. *J. Atmos. Oceanic Technol.*, **19**, 543–567.

Press, W. H., S. A. Teukolsky, W. T. Vetterling, and B. P. Flannery, 1992: *Numerical Recipes in FORTRAN: The Art of Scientific Computing*. 2nd ed. Cambridge University Press, 963 pp.

Protat, A., and I. Zawadzki, 2000: Optimization of dynamic retrievals from a multiple-Doppler radar network. *J. Atmos. Oceanic Technol.*, **17**, 753–760.

——, ——, and A. Caya, 2001: Kinematic and thermodynamic study of a shallow hailstorm sampled by the McGill bistatic multiple-Doppler radar network. *J. Atmos. Sci.*, **58**, 1222–1248.

Shapiro, A., S. Ellis, and J. Shaw, 1995: Single-Doppler velocity retrievals with Phoenix II data: Clear air and microburst wind retrievals in the planetary boundary layer. *J. Atmos. Sci.*, **52**, 1265–1287.

——, C. K. Potvin, and J. Gao, 2009: Use of a vertical vorticity equation in variational dual-Doppler wind analysis. *J. Atmos. Oceanic Technol.*, **26**, 2089–2106.

——, K. M. Willingham, and C. K. Potvin, 2010: Spatially variable advection correction of radar data. *J. Atmos. Sci*, in preparation.

Taylor, G. I., 1938: The spectrum of turbulence. *Proc. Roy. Soc. London*, **164A**, 476–490.

Xue, M., and Coauthors, 2001: The Advanced Regional Prediction System (ARPS)—A multi-scale nonhydrostatic atmospheric simulation and prediction tool. Part II: Model physics and applications. *Meteor. Atmos. Phys.*, **76**, 143–165.

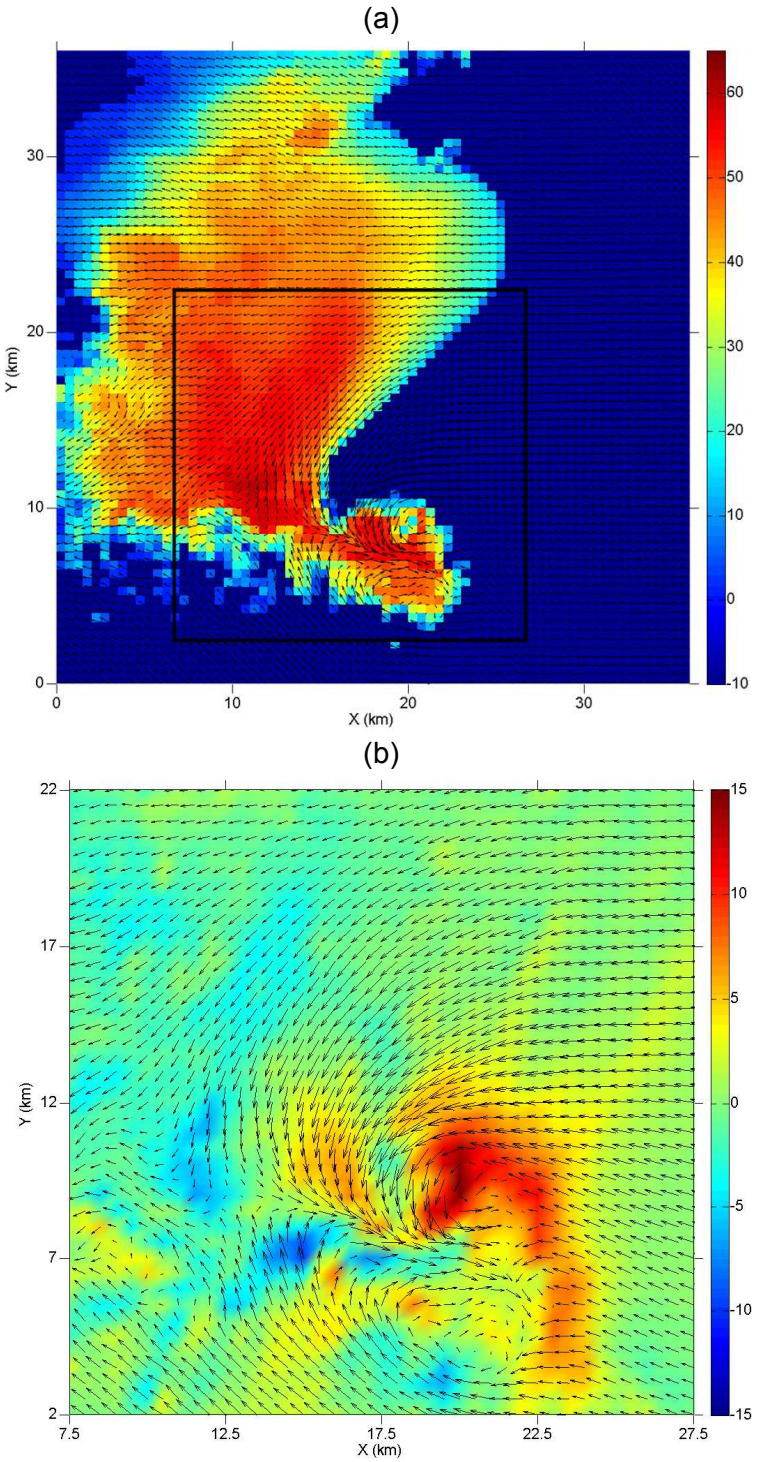

Figure 1. (a) Simulated reflectivity (dBZ) and horizontal wind vectors at z = 1 km. The box encloses the horizontal dual-Doppler analysis domain. (b) Simulated vertical velocity (m s^{-1}) and horizontal wind vectors over the analysis domain at z = 1 km.

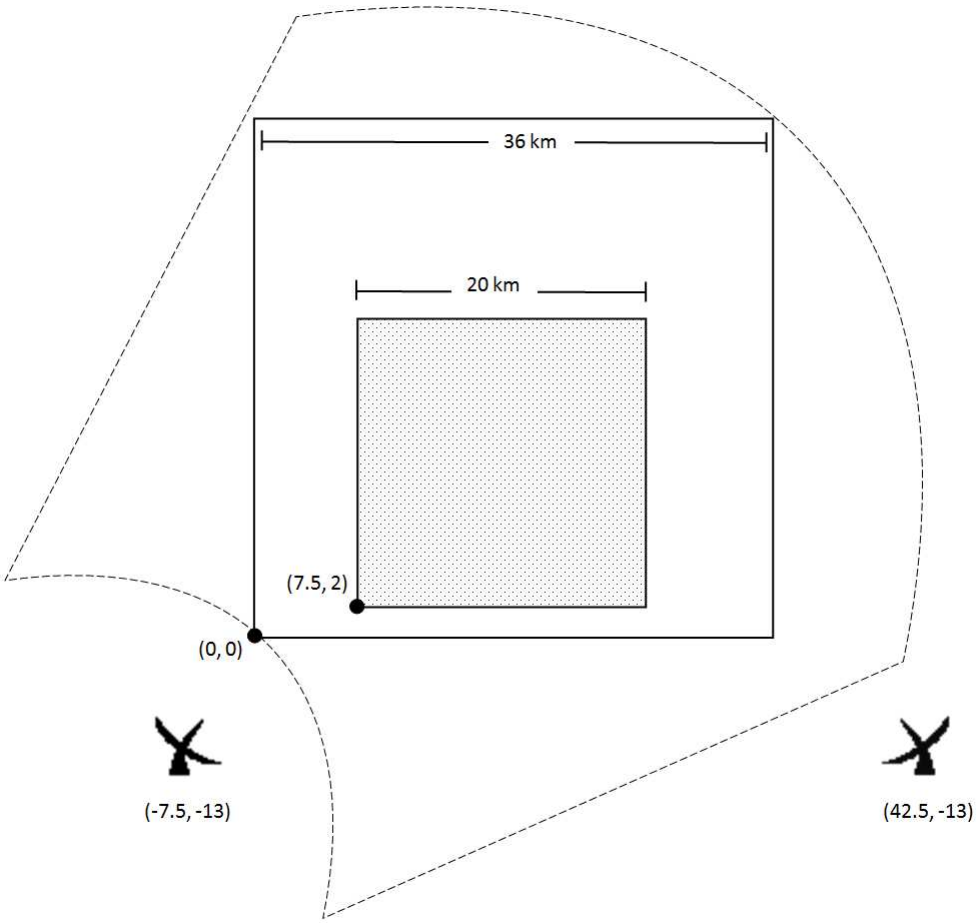

Figure 2. The analysis and radar domains.

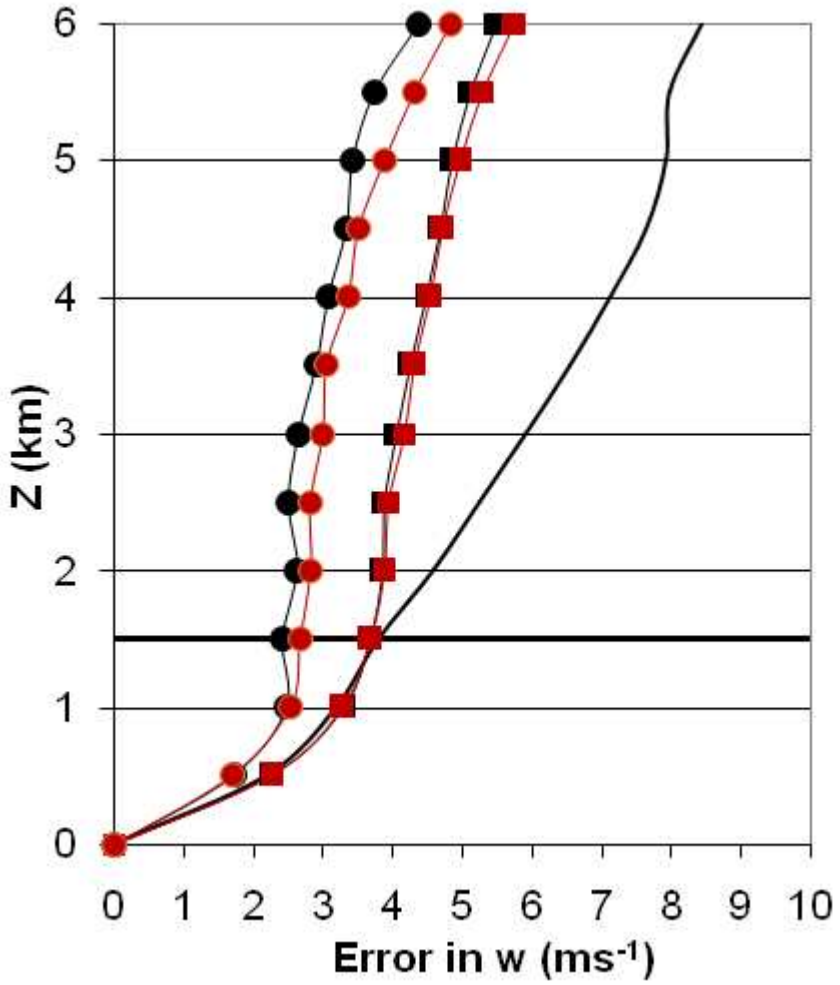

Figure 3. RMSE in *w* at each analysis level for VORT (circles) and NOVORT (squares) for volume scan times of 1 min (black) and 2 min (red). The RMS "true" *w* is represented by the plain curve. The bold horizontal line at *z* = 1.5 km represents the data cutoff level.

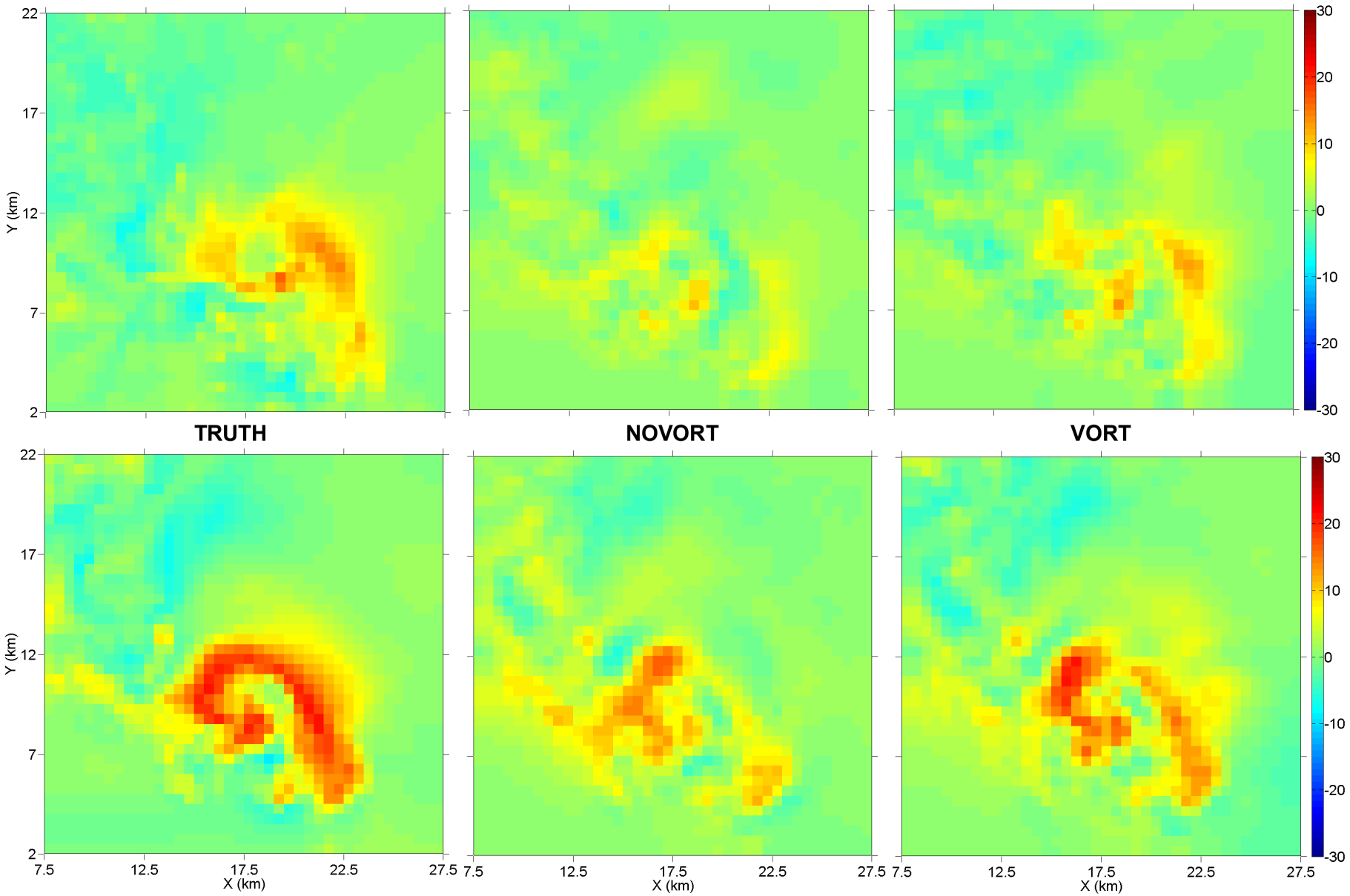

Figure 4. True, NOVORT and VORT *w* at *z* = 1.5 km (top) and *z* = 3 km (bottom).

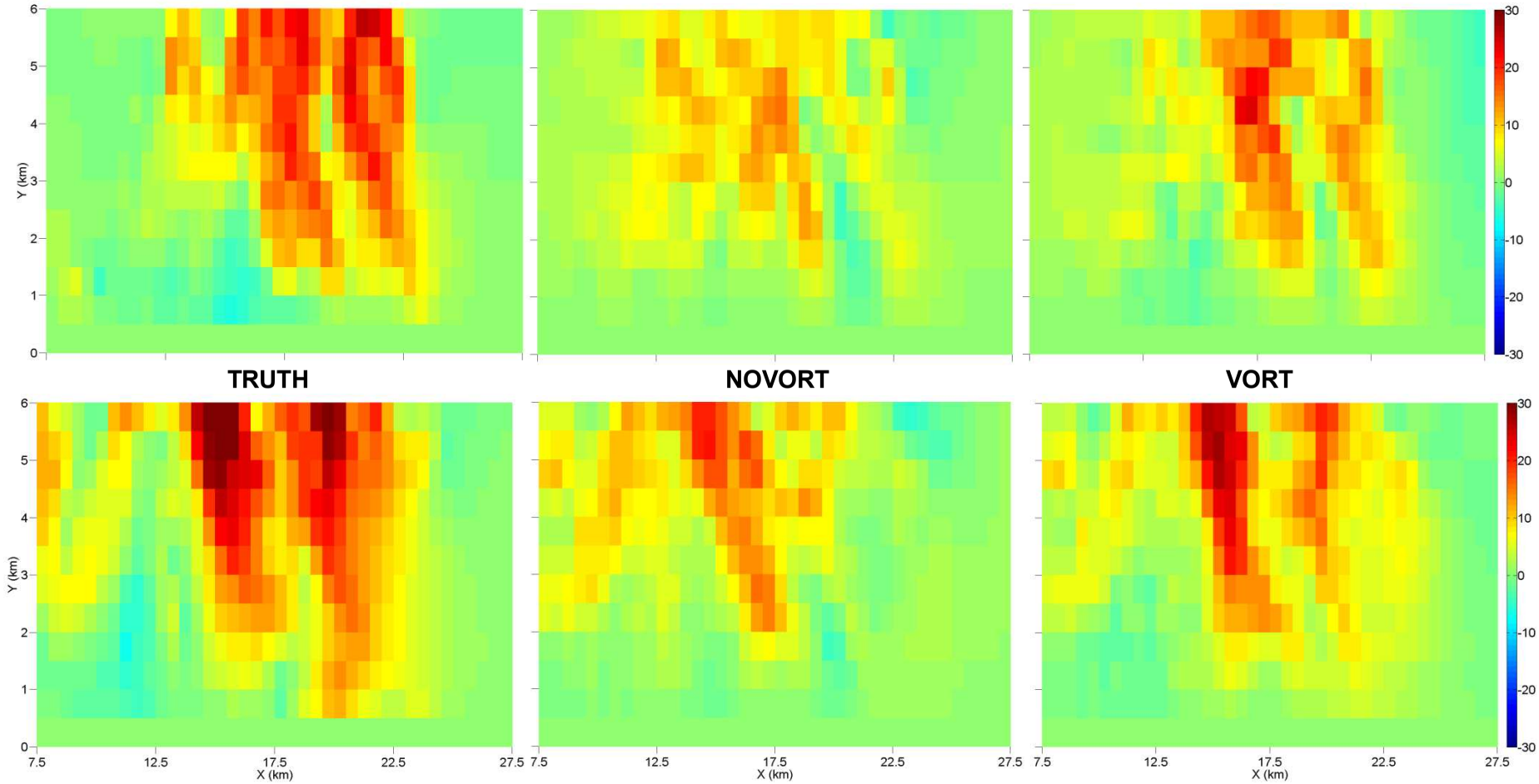

Figure 5. True, NOVORT and VORT *w* at *y* = 8 km (top) and *y* = 12.5 km (bottom).

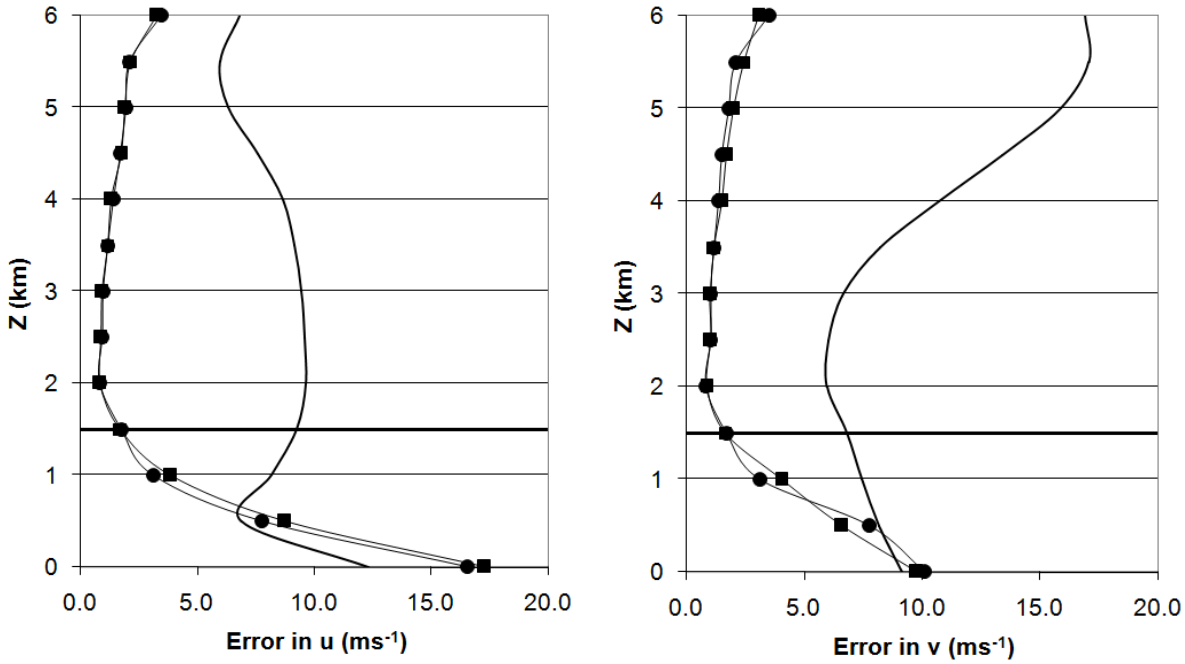

Figure 6. Same as Fig. 3 but for *u* and *v* for a volume scan time of 1 min.